Published in final edited form as:
Biochemistry. 2012 April 24; 51(16): 3433–3444. doi:10.1021/bi300197h.

The Catalytic Mechanism of Perosamine *N*-Acetyltransferase Revealed by High Resolution X-ray Crystallographic Studies and Kinetic Analyses[¶]

James B. Thoden[†], **Laurie A. Reinhardt**[†], **Paul D. Cook**[‡], **Patrick Menden**[§], **W. W. Cleland**[†,*], and **Hazel M. Holden**[†,*]

[†]Department of Biochemistry, University of Wisconsin, Madison, WI 53706

[‡]Department of Chemistry and Biochemistry, University of Mount Union, Alliance, OH 44601

[§]McArdle Laboratory for Cancer Research, University of Wisconsin School of Medicine and Public Health, Madison, WI 53706

Abstract

N-acetylperosamine is an unusual dideoxysugar found in the *o*-antigens of some Gram-negative bacteria including the pathogenic *Escherichia coli* strain O157:H7. The last step in its biosynthesis is catalyzed by PerB, an *N*-acetyltransferase belonging to the left-handed β-helix superfamily of proteins. Here we describe a combined structural and functional investigation on PerB from *Caulobacter crescentus*. For this study, three structures were determined to 1.0 Å resolution or better: the enzyme in complex with CoA and GDP-perosamine, the protein with bound CoA and GDP-*N*-acetylperosamine, and the enzyme containing a tetrahedral transition state mimic bound in the active site. Each subunit of the trimeric enzyme folds into two distinct regions. The N-terminal domain is globular and dominated by a six-stranded mainly parallel β-sheet. It provides most of the interactions between the protein and GDP-perosamine. The C-terminal domain consists of a left-handed β-helix, which has nearly seven turns. This region provides the scaffold for CoA binding. On the basis of these high-resolution structures, site-directed mutant proteins were constructed to test the roles of His 141 and Asp 142 in the catalytic mechanism. Kinetic data and pH rate profiles are indicative of His 141 serving as a general base. In addition, the backbone amide group of Gly 159 provides an oxyanion hole for stabilization of the tetrahedral transition state. The pH rate profiles are also consistent with the GDP-linked amino sugar substrate entering the active site in its unprotonated form. Finally, for this investigation, we show that PerB can accept GDP-3-deoxyperosamine as an alternative substrate, thus representing the production of a novel trideoxysugar.

[¶]This research was supported in part by NIH grants DK47814 (to H. M. H.) and GM18938 (to W. W. C).

[*]To whom correspondence should be addressed: Hazel_Holden@biochem.wisc.edu or cleland@biochem.wisc.edu, FAX: 608-262-1319, PHONE: 608-262-4988.

X-ray coordinates have been deposited in the Research Collaboratory for Structural Bioinformatics, Rutgers University, New Brunswick, N. J. (accession nos. 4EA7, 4EA8, 4EA9, 4EAA, 4EAB).

The authors have no competing financial interests.

Escherichia coli O157:H7 was first identified as a pathogenic organism in 1982 during two food poisoning outbreaks in Oregon and Michigan.[1] Since then, it has been shown to be the most common disease-causing *E. coli* strain in North America.[2] In 2006, for example, it was responsible for the spinach contamination that led to a massive infection outbreak.

The *O*-antigen of *E. coli* O157:H7 consists of a four sugar-repeating unit with the following structure: [→2-α-D-*N*-acetylperosamine-(1→3)-α-L-fucose-(1→4)-β-D-glucose-(1→3)-α-D-*N*-acetylgalactose→].[3] The *N*-acetylperosamine moiety is reasonably rare, but has also been identified in additional bacterial species including *Vibrio cholerae*, *Citrobacter youngae*, and *Caulobacter crescentus*, among others.[4-6]

The biosynthesis of *N*-acetylperosamine in both *E. coli* and *C. crescentus* involves four enzymatic steps starting with mannose-1-phosphate as highlighted in Scheme 1.[6,7] The first step involves the attachment of a GMP moiety to the sugar phosphate substrate. This reaction is catalyzed by mannose-1-phosphate guanylyltransferase. In the next step, GDP-mannose is converted to GDP-4-keto-6-deoxy-D-mannose by the action of GDP-mannose-4,6-dehydratase, an enzyme that has been well characterized both biochemically and structurally.[8-10] The third step of the pathway is catalyzed by GDP-perosamine synthase (PerA), a pyridoxal-5′-phosphate dependent enzyme belonging to the aspartate aminotransferase superfamily.[11-13] Completion of the pathway involves the acetylation of the sugar C-4‴ amino group by an *N*-acetyltransferase referred to as PerB.[6,7]

On the basis of amino acid sequence analyses, it is clear that PerB belongs to the left-handed β-helix family (LβH) of *N*-acetyltransferases. Members in this family are characterized by a left-handed β-helix, which was first observed in UDP-*N*-acetylglucosamine acyltransferase.[14] In recent years the three-dimensional structures of various *N*-acetyltransferases and *N*-acyltransferases functioning specifically on nucleotide-linked sugars have been reported.[15-24] Some of these enzymes acetylate the amino groups attached to C-3‴ of the hexose, whereas others operate on the amino groups at C-4‴ as in the case of PerB. Likewise, some have catalytic mechanisms that presumably involve a histidine serving as a general base, whereas others have active sites devoid of such residues.[24] It is thought in these enzymes that the sulfur of CoA ultimately serves as the catalytic base.[21] In all cases reported thus far, however, these enzymes function on either dTDP- or UDP-activated hexoses as opposed to PerB that utilizes a GDP-linked sugar as its substrate.

Here we present a combined structural and functional investigation of PerB from *C. crescentus*. For this study three crystal structures were determined to high resolution: the enzyme complexed with CoA and GDP-perosamine, the protein with bound CoA and GDP-*N*-acetylperosamine, and the enzyme in which a tetrahedral transition state analog was trapped in the active site. On the basis of these structures, site-directed mutant proteins of His 141 and Asp 142 were constructed to test their roles in catalysis. Both the kinetic analyses and pH rate profiles are consistent with His 141 serving as a general base in the reaction mechanism. In addition, the pH rate profiles suggest that the amino sugar enters the active site in an unprotonated form. The investigation described herein represents the first structural analysis of an *N*-acetyltransferase that employs a GDP-linked hexose as its substrate. More importantly, this study provides detailed molecular snapshots along the PerB

reaction mechanism from a pseudo Michaelis complex to a tetrahedral transition state mimic to a product complex.

Materials and Methods

Cloning, Expression, and Purification

Genomic DNA from *C. crescentus* was obtained from American Type Culture Collection. The *PerB* gene was PCR-amplified from genomic DNA such that the forward primer 5′-AAAA*CATATG*AGCGCTTCCCTCGCCATCGGGG and the reverse primer 5′-AAAA*CTCGAG*TCACGAACGGTCTCCTTTGATCTTGGCCGG added NdeI and XhoI cloning sites, respectively. The purified PCR product was A-tailed and ligated into a pGEM-T (Promega) vector for screening and sequencing. A PerB-pGEM-T vector construct of the correct sequence was then appropriately digested and ligated into a pET28(b_+) (Novagen) plasmid that had been previously modified to include a TEV cleavage site for protein production with an N-terminal His_6-tag.

The PerB-pET28 plasmid was used to transform Rosetta(DE3) *E. coli* cells (Novagen). The culture, in lysogeny broth, was grown at 37°C with shaking until the optical density at 600 nm reached 0.7. These cultures were then cooled in an ice water bath, induced with 1.0 mM isopropylthiogalactoside, and transferred to a refrigerated shaker at 16°C. The cells were allowed to express protein at 16°C for 24 hours after induction. PerB was purified by standard procedures using Ni-nitrilotriacetic acid resin. Following purification, the protein was dialyzed against 10 mM Tris and 200 mM NaCl at pH 8.0, and then concentrated to 2 mg/ml.

Structural Analysis of PerB

Crystallization conditions were initially surveyed via the hanging drop method of vapor diffusion and using a sparse matrix screen developed in the laboratory. Experiments were conducted with the apoprotein, with protein in the presence of 5 mM acetyl CoA and with protein in the presence of 5 mM CoA and 5 mM GDP. Small crystals were obtained under a number of conditions from pH 6 - 8 with various poly(ethylene glycols) serving as precipitants. The limited solubility of the protein, however, precluded the growth of suitable X-ray diffraction quality crystals.

Attempts to remove the N-terminal His_6-tag by TEV protease were unsuccessful. In addition, cloning PerB into expression vectors to yield an enzyme with no His_6-tag or a C-terminally tagged version yielded protein that either did not express well or that was even less soluble.

In order to make the TEV cleavage site more accessible, the pET28 construct was modified via mutagenesis such that three alanine residues were introduced between Met 1 and Ser 2. This protein was expressed as previously described and was purified by modifications to the standard procedures at room temperature using Ni-nitrilotriacetic acid resin. Specifically, all buffers contained 500 mM NaCl and, additionally, 10% glycerol. Purified protein was dialyzed against 10 mM Tris (pH 8) with 500 mM NaCl and 10% glycerol, and subsequently digested with TEV protease at a molar ratio of 1:30 at room temperature for 24 hours. The

TEV protease and small amounts of non-cleaved protein were removed by passing the digested mixture over nitrilotriacetic acid resin. The cleaved protein was pooled and dialyzed two times against 4 L of 10 mM Tris (pH 8) with 500 mM NaCl, and then concentrated to 10 mg/ml, based on a calculated extinction constant of 3.66 $(mg/mL)^{-1}$ cm^{-1}.

Enzymatic activity of the modified protein was verified by its ability to convert GDP-perosamine to GDP-*N*-acetylperosamine with acetyl CoA. A 1 mL reaction buffered at pH 8.0 with 50 mM HEPPS containing 1.0 mM acetyl CoA, 1.0 mM GDP-perosamine, and 0.2 mg/mL PerB was incubated at room temperature for 2 hr. The reaction products were separated from the protein by filtration through a 10 kDa ultrafiltration membrane, diluted with two volumes of water, and loaded onto a 1 mL Resource-Q column. Elution with a 20 mL gradient at pH 4 from 0 to 2.25 M ammonium acetate showed the elimination of the GDP-perosamine starting material (retention 7.4 mL) and the generation of a new peak with a retention volume of 12.3 mL. The identity of this peak as GDP-*N*-acetylperosamine was verified by ESI mass spectrometry (Mass Spectrometry/Proteomic Facility at the University of Wisconsin). The GDP-perosamine required for the assay was prepared as previously described.[13]

Crystallization conditions for modified PerB were again surveyed via the hanging drop method of vapor diffusion with either the apoprotein or protein incubated with 5 mM CoA and 5 mM GDP. X-ray diffraction quality crystals were subsequently grown by mixing in a 1:1 ratio the protein incubated with CoA and GDP and 24-30% monomethylether poly(ethylene glycol) 5000 at pH 7.5. These crystals grew to maximal dimensions of 0.8 × 0.8 × 0.4 mm and belonged to the space group I23 with unit cell dimensions of $a = b = c =$ 115.0 Å. The asymmetric unit contained one subunit.

Prior to X-ray data collection, all crystals were transferred to a cryoprotectant solution containing 30% monomethylether poly(ethylene glycol) 5000, 600 mM NaCl, 5 mM GDP, 5 mM CoA, and 12% ethylene glycol. The PerB structure was initially solved by single isomorphous replacement using a crystal complexed with GDP and CoA and soaked in a solution containing 1 mM methylmercury acetate for one day. X-ray data sets from crystals of the native protein or the native protein soaked in mercury were measured at 100 K using a Bruker AXS Platinum 135 CCD detector controlled with the Proteum software suite (Bruker AXS Inc.). The X-ray source was Cu Kα radiation from a Rigaku RU200 X-ray generator equipped with Montel optics and operated at 50 kV and 90 mA. These X-ray data were processed with SAINT version 7.06A (Bruker AXS Inc.) and internally scaled with SADABS version 2005/1 (Bruker AXS Inc.). Four mercury binding sites were identified with the program SOLVE,[25] giving an overall figure-of-merit of 0.33 to 1.7 Å resolution. Solvent flattening with RESOLVE[26,27] generated an interpretable electron density map, which allowed for a preliminary model to be constructed using the software package COOT.[28] This structure, refined with REFMAC,[29] served as the search model for the subsequent structural analyses of the various complexes described below via molecular replacement with the software package PHASER.[30]

All point mutations of the modified PerB-pET28 plasmid construct were created via the Stratagene QuikChange method and sequenced to verify that no other changes had been

introduced into the gene. The three mutant proteins that were studied, H141N, H141A, and D142N, were expressed and purified in the same manner as that for the wild-type enzyme. Two of the proteins, H141N and H141A, were crystallized and X-ray data sets from these crystals were also collected using “in-house” equipment. These structures were refined with REFMAC.[29] X-ray data collection and relevant refinement statistics for these mutant protein structures are presented in Tables 1 and 2, respectively.

Three different ultra high-resolution complexes were subsequently prepared for this investigation. The first was that of the enzyme with bound CoA and GDP-perosamine. For this complex, wild-type crystals were soaked overnight in a synthetic mother liquor containing 5 mM CoA and 20 mM GDP-perosamine. The second complex was that of PerB in the presence of CoA and GDP-*N*-acetylperosamine. Wild-type crystals were soaked in a synthetic mother liquor containing 10 mM acetyl CoA and 10 mM GDP-perosamine for six hours. The enzyme turned over, and CoA and GDP-*N*-acetylperosamine were left bound in the active site. For preparation of the transition state (or intermediate) analog, the enzyme was co-crystallized in the presence of 10 mM CoA and 10 mM GDP-perosamine. Note that all crystals were grown at room temperature, and small crystals typically appeared within one day. Crystal growth was generally completed within two weeks.

High-resolution X-ray data sets from flash-cooled crystals of these three complexes were collected at the Structural Biology Center Beamline 19-ID at a wavelength of 0.667 Å (Advanced Photon Source, Argonne National Laboratory, Argonne, IL). The X-ray data sets were processed and scaled with HKL3000.[31] X-ray data collection statistics are presented in Table 1. These structures were initially refined with REFMAC.[29] After major changes and most solvent molecules were identified, the structures were then subjected to restrained conjugate gradient least squares with SHELXL-97.[32] All non-hydrogen atoms were refined with anisotropic thermal parameters, and hydrogen atoms were included in the final rounds of refinement in their idealized positions for all protein and ligand atoms.

Measurement of the Kinetic Constants for the Wild-type Enzyme and the Site-Directed Mutant Proteins

The kinetic constants for the wild-type PerB and the site-directed mutant proteins were determined via a discontinuous assay using an ÄKTA HPLC system equipped with a 1 mL Resource-Q column. The reaction rates were determined by calculating the amount of GDP-*N*-acetylperosamine produced on the basis of the peak area in the HPLC trace. The area was correlated to concentration via a calibration curve created with standard samples that had been treated in the same manner as the reaction aliquots.

To determine the kinetic parameters for the wild-type enzyme at pH 8, nine reactions were analyzed. The GDP-perosamine concentrations were varied from 0.14 mM to 5.0 mM at a constant acetyl CoA concentration of 2.76 mM, whereas the acetyl CoA concentrations were varied from 0.07 mM to 2.76 mM at a constant GDP-perosamine concentration of 5.0 mM. All experiments were performed at 25°C and each 550 μL reaction was initiated by the addition of enzyme to a final concentration of 45 μg/mL. For each reaction, 100 μL aliquots were taken at time zero and at 1-2 minute intervals over a span of eight minutes. The individual aliquots were immediately quenched by the addition of 6 μL of 6 M HCl.

Subsequently, 40 μL of CCl_4 was added to each sample, which was then vortexed and centrifuged for 1 min to remove denatured protein. An 80 μL aliquot of the aqueous phase was taken from each sample and diluted with 600 μL of water, and 500 μL of this solution was loaded onto the Resource-Q column for analysis. All HPLC analyses were performed using solutions at pH 4 and a gradient of 0 to 2.25 M ammonium acetate.

A plot of concentration versus time was generated for each reaction, which allowed for initial rates to be determined. All data points were fitted to the following equation:

$$v=VAB/(K_aB+K_bA+K_{ia}K_b+AB)$$

using SigmaPlot8, where K_a and K_b were the Michaelis constants for GDP-perosamine and acetyl CoA, respectively, and V was the maximum velocity.

For determination of pH rate profiles, reactions were conducted using the following buffers at concentrations of 200 mM: MES (pH 6), MOPS (pH 7), HEPPS (pH 8), CHES (pH 9), CAPS (pH 10 and 11). The wild-type enzyme and the three mutant proteins were analyzed in a similar manner as described above. The concentrations of the substrates and enzymes were varied as needed as well as the reaction times in order to obtain linear plots from which to determine the initial velocities. Note that the acetyl CoA binding constants were essentially unaffected by changes in pH (unpublished data).

The pK_a values were obtained by fitting the data to the appropriate equations using the programs BELL (equation 1) or BEL2L (equation 2).[33] The pH rate profile with an initial slope of 1 and final slope of -1 were fit with equation 1. The pH rate profiles with an initial slope of 2 and final slope of -1 were fit with equation 2.

$$\log y=\log(C/(1+H/K_1+K_2/H)) \quad (1)$$

$$\log y=\log(C/(1+H/K_1+K_2/H+H^2/K_3)) \quad (2)$$

All kinetic data are provided in Tables 3, 4 and 5.

Production of GDP-*N*-acetyl-3-deoxyperosamine

GDP-3-deoxyperosamine was produced as described elsewhere.[13] For the production of GDP-*N*-acetyl-3-deoxyperosamine, the typical reactions contained 2 mM GDP-3-deoxyperosamine, 1 mM acetyl CoA, and 10 μM PerB in 50 mM HEPES (pH 7.5), 50 mM NaCl, and 10 mM $MgCl_2$. The reactions were carried out for 2-4 hours at room temperature, after which they were filtered through a 10 kDa Amicon filter to remove the protein. The reactions were then analyzed via HPLC by loading them onto a 1 mL Resource-Q (G.E. Healthcare) anion exchange column equilibrated with 20 mM ammonium bicarbonate. Reaction components were eluted with a linear gradient to 50% with 500 mM ammonium bicarbonate, and the fraction(s) were analyzed by ESI mass spectrometry and ^1H NMR (in D_2O).

Results and Discussion

Overall Structure of PerB in Complex with CoA and the GDP-perosamine Substrate (pseudo Michaelis complex)

The crystals used for this analysis diffracted to 1.0-Å resolution and belonged to the space group I23. PerB functions as a trimer, and in this crystal form the biological unit packed along a crystallographic three-fold rotational axis resulting in one subunit per asymmetric unit. Each subunit of the trimer contains 215 amino acid residues.[6] With the exception of the first two N-terminal residues, the loop between Pro 41 and Arg 43, and the final three C-terminal residues, the electron density corresponding to the polypeptide chain backbone was well ordered. The Ramachandran plot statistics for the model, as calculated with PROCHECK,[34] were excellent with 90.4% and 9.6% of the ϕ,ψ angles lying within the core and allowed regions, respectively.

A ribbon representation of the PerB trimer is shown in Figure 1a. It has overall dimensions of 70 Å × 70 Å × 70 Å, and as can be seen the active sites of the trimer are wedged between subunits. A stereo view of an individual subunit is presented in Figure 1b. The subunit can be envisioned in terms of two domains, an N-terminal globular motif delineated by Ala 3 to Leu 93 and a β-helical region formed by Val 94 to the C-terminus. The N-terminal domain contains a six-stranded mostly parallel β-sheet flanked on one side by two α-helices and on the other by a single α-helix. The first α-helix of the subunit is situated such that the positive end of its helix dipole moment points towards the pyrophosphoryl moiety of GDP-perosamine. The sixth β-strand of the N-terminal domain serves as a bridge to the β-helix domain, which contains nearly seven turns and displays the characteristic hexapeptide repeat that is a hallmark for this family of *N*-acetyltransferases.[35] Whereas the N-terminal domain provides most of the interactions between the protein and the GDP-perosamine ligand, the C-terminal domain serves to anchor the CoA moiety into the active site. Pro 207 adopts the *cis* conformation and is situated near the adenine ring of CoA.

Electron density corresponding to the bound ligands is presented in Figure 2a. The density for the CoA is very strong, as is that for the GDP portion of the substrate. The electron density for the hexose portion of GDP-perosamine is somewhat weaker, however. This most likely is a result of the short crystal soaking times employed for this structural analysis. As discussed below, if the PerB crystals were soaked in CoA and GDP-perosamine for extended periods of time, a covalent adduct formed between the two ligands.

A close-up view of the CoA binding pocket is provided in Figure 2b. The cofactor is anchored in place simply by water molecules, the backbone amide groups of Val 171 and Ala 189, and the carbonyl group of Ala 189. The sulfur of CoA lies at 3.6 Å from the sugar C-4‴ amino group. The protein region surrounding the GDP-perosamine ligand is displayed in Figure 2c. The guanine base is held in place by two water molecules, the carboxylate side chain of Asp 55, and the carbonyl group of Val 37. The carboxylate group of Asp 38 bridges the ribose C-2′ and C-3′ hydroxyls. In addition to numerous water molecules, the backbone amide groups of Gly 17, His 18, and Gly 74 participate in hydrogen bonding interactions with the phosphoryl oxygens. With the exception of His 141, the hexose moiety of GDP-perosamine does not interact with protein backbone atoms or side chain groups but rather

simply with water molecules. His 141, which is provided by a neighboring subunit, is positioned at 2.7 Å from the hexose C-4‴ amino group.

Given the lack of protein side chain interactions between PerB and the hexose moiety of GDP-perosamine, we were curious as to whether we could produce a novel trideoxysugar. In a previous study, we were able synthesize via enzymatic means, GDP-3-deoxyperosamine, which is not found in nature. Using GDP-3-deoxyperosamine, we were able to, indeed, show that PerB produces an acetylated form of the sugar. Specifically, the ESI mass spectrum corresponding to a fraction from the HPLC purification containing a GDP-sugar showed a peak at 629 amu, which is the appropriate mass for GDP-*N*-acetyl-3-deoxyperosamine. The ^{1}H NMR spectrum for the compound isolated from the above mentioned fraction (in D_2O) is shown in Figure 3. This spectrum corresponds closely to the ^{1}H NMR spectrum for GDP-3-deoxyperosamine, but with the addition of the peak near 1.8 ppm, which is the appropriate chemical shift for protons in an *N*-acetyl group.

Overall Structure of PerB in Complex with CoA and the *GDP-N*-acetylperosamine product

The next structure determined in this study was that of PerB complexed with CoA and GDP-*N*-acetylperosamine. As in the previously described PerB/CoA/GDP-perosamine structure, the crystals employed in this analysis also belonged to the space group I23 with one subunit in the asymmetric unit. The structure was solved to a nominal resolution of 1.0 Å and, again, 90.4% and 9.6% of the ϕ, ψ angles for the model were found to lie within the core and allowed regions, respectively, of the Ramachandran plot. There were no major conformational changes that occurred upon the binding of GDP-*N*-acetylperosamine versus GDP-perosamine. Indeed, the α-carbons for the two protein models superimpose with a root-mean-square deviation of 0.13 Å.

The electron densities corresponding to CoA and GDP-*N*-acetylperosamine are presented in Figures 4a and 4b. As can be seen, the acetylated nucleotide-linked sugar product has clearly been trapped in the active site cleft. To the best of our knowledge, this is the first time an *N*-acetylated sugar product has been observed in the active site of any *N*-acetyltransferase that functions on nucleotide-linked sugars.

The local area surrounding the acetylated sugar is displayed in Figure 4c. His 141 shifts slightly in the active site so that it no longer interacts with the sugar amino nitrogen but rather with the C-3‴ hydroxyl group. The backbone amide group of Gly 159 lies within hydrogen bonding distance (3.0 Å) to the carbonyl oxygen of the acetyl moiety. Both His 141 and Gly 159 are provided by a neighboring subunit in the trimer.

Overall Structure of PerB in Complex with a Transition State Mimic

When PerB was co-crystallized in the presence in CoA and GDP-perosamine, a covalent adduct formed that bridged the sulfur of CoA and the amino nitrogen of GDP-perosamine as can be seen in the electron density map calculated to 0.9-Å resolution (Figure 5a). Given the high resolution of this structure, and the observed bond lengths, we believe this crosslinking group is $CHCH_3$. The hybridization about the linking carbon is clearly sp^3. The question thus arises as to how this adduct was formed. The crystals were grown in the presence of

polyethylene glycol, and commercial samples of it are notorious for being contaminated with peroxides, aldehydes, and aldehyde precursors.[36] A possible mechanism for the crosslinking of CoA and GDP-perosamine is shown in Scheme 2. We suggest that the C-4‴ amino group attacks the carbonyl carbon of acetaldehyde to form a tetrahedral intermediate. This intermediate collapses to produce a Schiff base, which is subsequently attacked by the sulfhydryl group of CoA. Clearly PerB can accommodate acetaldehyde in the region between the CoA sulfur and the sugar nitrogen because it has to bind acetyl CoA for catalysis to ultimately occur.

A close-up view of the PerB active site with the bound CoA/GDP-perosamine adduct is displayed in Figure 5b. His 141 is positioned within 3.0 Å of the sugar nitrogen. The models of PerB with bound GDP-*N*-acetylperosamine or the covalent adduct are virtually identical such that their α-carbons superimpose with a root-mean-square deviation of 0.11 Å. The covalent adduct shown in Figure 5b serves as an excellent mimic for the tetrahedral transition state that would occur as the sugar amino nitrogen attacks the carbonyl carbon of acetyl CoA. The only difference is that the proton on the bridging carbon would be an oxygen atom in the true tetrahedral intermediate. Given that, a model for the tetrahedral intermediate was created and is shown in Figure 5c superimposed upon the structure of the enzyme with bound GDP-*N*-acetylperosamine. The acetyl carbon moves by ∼0.7 Å in the active site upon collapse of the tetrahedral intermediate. Most likely the backbone amide of Gly 159 provides stabilization of the oxyanion that forms during the reaction mechanism.

Probing the Catalytic Mechanism of PerB

The closest structural relative to PerB is an *N*-acetyltransferase referred to as PlgD from *Campylobacter jejuni*.[19,20] It catalyzes the last step in the biosynthesis of 2,4-diacetamido-2,4,6-trideoxy-α-D-glucose, an unusual sugar found in the glycan moieties of some eubacterial pathogens, and it employs a UDP-linked sugar substrate. PerB and PglD show an amino acid sequence identity of 38%, and, not surprisingly, their models superimpose with a root-mean-square deviation of 0.73 Å for 157 structurally equivalent α-carbon positions. A superposition of the PerB active site onto that of PlgD is presented in Figure 6. There are two substitutions in PglD, relative to PerB, which preclude its ability to bind a GDP-linked sugar substrate. One is Tyr 10 that is an isoleucine (Ile 13) in PerB. The second is Asp 36, which in PerB corresponds to Ala 39.

It has been proposed for PglD that His 125, the structural equivalent of His 141 in PerB, functions as the active site base. In addition, it is believed that Glu 126 (Asp 142 in PerB) serves to increase the basicity of the His 125 imidazole. To test the roles of these residues in the PerB mechanism, three site-directed mutant proteins were constructed: H141N, H141A, and D142N. Both their kinetic parameters and pH rate profiles were measured and compared to those of the wild-type enzyme (Tables 3, 4, and 5). In addition, the structures of the H141N and H141A mutant proteins were determined to 1.45-Å and 1.35-Å resolution, respectively. These structures demonstrated that no substantial conformational changes occurred because of the mutations, and that the differences in the observed kinetic parameters are simply due to the loss of the imidazole side chain of His 141. Indeed, the α-

carbons for the H141N and H141A models superimpose upon those of the wild-type enzyme with a root-mean-square deviation of 0.08 Å.

The wild-type enzyme shows a K_m for GDP-perosamine of 0.087 ± 0.011 mM, a K_m for acetyl CoA of 0.15 ± 0.02 mM, and a catalytic efficiency of 3.4×10^6 $M^{-1}s^{-1}$. When His 141 is changed to an asparagine residue, the K_m values for GDP-perosamine and acetyl CoA are not altered to any great extent (Table 3). Importantly, however, the catalytic efficiency drops by over four orders of magnitude. Likewise, the H141A mutant protein demonstrates only slight alterations in the K_m values for GDP-perosamine and acetyl CoA, but the catalytic efficiency drops by six orders of magnitude. This behavior is characteristic for a general base. The substitution of Asp 142 with an asparagine residue results in an order of magnitude lower catalytic efficiency suggesting that it probably plays a role in positioning His 141.

In the pH rate profiles of V_{max}/K_m, the pK_{a2} at 9.3 for the wild-type enzyme is most certainly the pK_a of the amino sugar substrate (Table 5). Why do we believe this to be the case? Consider the pK_a of 2-amino-1,3-propandiol, which is 8.8. This compound mimics the C-3‴-C-5‴ region of the GDP-linked sugar substrate. In addition, the negative charges on the pyrophosphoryl portion of the GDP-perosamine substrate would be expected to raise its pK_a by ∼0.4 units to 9.2 (by analogy to the change from glucosamine with a pK_a 7.8 to glucosamine-6-phosphate with a pK_a 8.2).[37] It is not clear, however, what group on the enzyme is responsible for the pK_{a1} around 8 in the pH rate profile of V_{max}/K_m. It cannot be His 141, as the profile still shows this pK_a with the H141N mutant, so presumably the pK_a of His 141 is significantly less than 8.

There are two possible interpretations of the pH rate profiles. One scenario is that the substrate binds in the PerB active site with its amino group protonated. His 141 then functions to remove this proton so the free electron pair can then attack the carbonyl group of acetyl CoA. This is the mechanism proposed by Olivier and Imperiali.[20] The group with the pK_a ∼8 must thus be in its ionized form. Another interpretation of the pH rate profiles is that a reverse protonation mechanism is occurring with the substrate binding in the active site as a neutral amine, and the group with the pK_a ∼8 reacting in its protonated form. The role of His 141 would then be to act as a general base to remove one of the remaining protons from the amino group of the substrate as it attacks acetyl CoA.

Both of these mechanisms are consistent with the pH profiles, but the second allows His 141 to act in a truly catalytic manner. In the first mechanism, His 141 only deprotonates the substrate to its neutral form, but there is then no catalysis of the transacylation reaction itself. In the second mechanism, His 141 acts as a general base to catalyze the formation of the tetrahedral transition state or intermediate, and thus it is expected that its mutation would have a major effect as observed. We thus conclude that the pH rate profiles are reverse protonation ones, and that the substrate enters the active site with a neutral amino group. The mechanism for PglD proposed by Rangarajan[19] also assumes that the substrate binds to the enzyme in its neutral state. A possible reaction mechanism for PerB is shown in Scheme 3. The key players in the mechanism include the backbone amide of Gly 159, which provides an “oxyanion” hole, and the imidazole of His 141, which serves as the general base.

The catalytic mechanisms of PglD and PerB clearly involve a general base provided by a histidine residue. This is in marked contrast to the reaction mechanisms of WlbB, QdtC, and AntD, which are *N*-acetyl or *N*-acyltransferases that have also been studied in our laboratory.[21-23] Both WlbB and QdtC are involved in the biosynthesis of unusual acetylated sugars found in the *O*-antigens of certain Gram-negative bacteria, and both function on C-3‴ hexose amino groups. AntD is involved in the production of D-anthrose, an important carbohydrate found in the endospores of *Bacillus anthracis*, the causative agent of anthrax. Specifically, AntD catalyzes the transfer of an acyl group from 3-hydroxy-3-methylbutyryl-CoA to the C-4‴ amino group of dTDP-4-amino-4,6-dideoxy-α-D-glucose. In all three enzymes, there is a decided lack of a catalytic base in their active sites. Likewise, in all three enzymes the nucleotide-linked sugars are bound similarly, but in a completely different orientation than that observed for PerB and PglD. Clearly the *N*-acetyltransferases (or *N*-acyltransferases) that function on nucleotide-linked sugars have evolved into two separate protein classes that differ with respect to both substrate binding orientations and reaction mechanisms.

Acknowledgments

A portion of the research described in this paper was performed at Argonne National Laboratory, Structural Biology Center at the Advanced Source (U. S. Department of Energy, Office of Biological and Environmental Research, under Contract DE-AC02-06CH11357). We gratefully acknowledge Dr. Norma E. C. Duke and Dr. Stephan L. Ginell for assistance during the X-ray data collection at Argonne.

References

1. Wells JG, Davis BR, Wachsmuth IK, Riley LW, Remis RS, Sokolow R, Morris GK. Laboratory investigation of hemorrhagic colitis outbreaks associated with a rare *Escherichia coli* serotype. Journal of clinical microbiology. 1983; 18:512–520. [PubMed: 6355145]
2. Mead PS, Griffin PM. *Escherichia coli* O157:H7. Lancet. 1998; 352:1207–1212. [PubMed: 9777854]
3. Perry MB, MacLean L, Griffith DW. Structure of the O-chain polysaccharide of the phenol-phase soluble lipopolysaccharide of *Escherichia coli* 0:157:H7. Biochem Cell Biol. 1986; 64:21–28. [PubMed: 3008786]
4. Haishima Y, Kondo S, Hisatsune K. The occurrence of alpha (1----2) linked *N*-acetylperosamine--homopolymer in lipopolysaccharides of non-O1 *Vibrio cholerae* possessing an antigenic factor in common with O1 *V. cholerae*. Microbiology and immunology. 1990; 34:1049–1054. [PubMed: 2098633]
5. Ovchinnikova OG, Kocharova NA, Katzenellenbogen E, Zatonsky GV, Shashkov AS, Knirel YA, Lipinski T, Gamian A. Structures of two *O*-polysaccharides of the lipopolysaccharide of *Citrobacter youngae* PCM 1538 (serogroup O9). Carbohydr Res. 2004; 339:881–884. [PubMed: 14980832]
6. Awram P, Smit J. Identification of lipopolysaccharide *O* antigen synthesis genes required for attachment of the *S*-layer of *Caulobacter crescentus*. Microbiology. 2001; 147:1451–1460. [PubMed: 11390676]
7. Albermann C, Beuttler H. Identification of the GDP-*N*-acetyl-d-perosamine producing enzymes from *Escherichia coli* O157:H7. FEBS Lett. 2008; 582:479–484. [PubMed: 18201574]
8. Somoza JR, Menon S, Schmidt H, Joseph-McCarthy D, Dessen A, Stahl ML, Somers WS, Sullivan FX. Structural and kinetic analysis of *Escherichia coli* GDP-mannose 4,6 dehydratase provides insights into the enzyme's catalytic mechanism and regulation by GDP-fucose. Structure Fold Des. 2000; 8:123–135. [PubMed: 10673432]

9. Mulichak AM, Bonin CP, Reiter WD, Garavito RM. Structure of the MUR1 GDP-mannose 4,6-dehydratase from *Arabidopsis thaliana*: implications for ligand binding and specificity. Biochemistry. 2002; 41:15578–15589. [PubMed: 12501186]
10. Webb NA, Mulichak AM, Lam JS, Rocchetta HL, Garavito RM. Crystal structure of a tetrameric GDP-D-mannose 4,6-dehydratase from a bacterial GDP-D-rhamnose biosynthetic pathway. Protein Sci. 2004; 13:529–539. [PubMed: 14739333]
11. Albermann C, Piepersberg W. Expression and identification of the RfbE protein from *Vibrio cholerae* O1 and its use for the enzymatic synthesis of GDP-d-perosamine. Glycobiology. 2001; 11:655–661. [PubMed: 11479276]
12. Zhao G, Liu J, Liu X, Chen M, Zhang H, Wang PG. Cloning and characterization of GDP-perosamine synthetase (Per) from *Escherichia coli* O157:H7 and synthesis of GDP-perosamine *in vitro*. Biochem Biophys Res Commun. 2007; 363:525–530. [PubMed: 17888872]
13. Cook PD, Holden HM. GDP-perosamine synthase: structural analysis and production of a novel trideoxysugar. Biochemistry. 2008; 47:2833–2840. [PubMed: 18247575]
14. Raetz CR, Roderick SL. A left-handed parallel beta helix in the structure of UDP-*N*-acetylglucosamine acyltransferase. Science. 1995; 270:997–1000. [PubMed: 7481807]
15. Brown K, Pompeo F, Dixon S, Mengin-Lecreulx D, Cambillau C, Bourne Y. Crystal structure of the bifunctional *N*-acetylglucosamine 1-phosphate uridyltransferase from *Escherichia coli*: a paradigm for the related pyrophosphorylase superfamily. EMBO J. 1999; 18:4096–4107. [PubMed: 10428949]
16. Olsen LR, Roderick SL. Structure of the *Escherichia coli* GlmU pyrophosphorylase and acetyltransferase active sites. Biochemistry. 2001; 40:1913–1921. [PubMed: 11329257]
17. Kostrewa D, D'Arcy A, Takacs B, Kamber M. Crystal structures of *Streptococcus pneumoniae N*-acetylglucosamine-1-phosphate uridyltransferase, GlmU, in apo form at 2.33 A resolution and in complex with UDP-*N*-acetylglucosamine and Mg(2+) at 1.96 Å resolution. J Mol Biol. 2001; 305:279–289. [PubMed: 11124906]
18. Sulzenbacher G, Gal L, Peneff C, Fassy F, Bourne Y. Crystal structure of *Streptococcus pneumoniae N*-acetylglucosamine-1-phosphate uridyltransferase bound to acetyl-coenzyme A reveals a novel active site architecture. J Biol Chem. 2001; 276:11844–11851. [PubMed: 11118459]
19. Rangarajan ES, Ruane KM, Sulea T, Watson DC, Proteau A, Leclerc S, Cygler M, Matte A, Young NM. Structure and active site residues of PglD, an *N*-acetyltransferase from the bacillosamine synthetic pathway required for *N*-glycan synthesis in *Campylobacter jejuni*. Biochemistry. 2008; 47:1827–1836. [PubMed: 18198901]
20. Olivier NB, Imperiali B. Crystal structure and catalytic mechanism of PglD from *Campylobacter jejuni*. J Biol Chem. 2008; 283:27937–27946. [PubMed: 18667421]
21. Thoden JB, Cook PD, Schaffer C, Messner P, Holden HM. Structural and functional studies of QdtC: an *N*-acetyltransferase required for the biosynthesis of dTDP-3-acetamido-3,6-dideoxy-alpha-d-glucose. Biochemistry. 2009; 48:2699–2709. [PubMed: 19191736]
22. Thoden JB, Holden HM. Molecular structure of WlbB, a bacterial *N*-acetyltransferase involved in the biosynthesis of 2,3-diacetamido-2,3-dideoxy-d-mannuronic acid. Biochemistry. 2010; 49:4644–4653. [PubMed: 20433200]
23. Kubiak RL, Holden HM. Structural Studies on AntD: an *N*-Acyltransferase Involved in the Biosynthesis of d-Anthrose. Biochemistry. 2012 online.
24. Holden HM, Cook PD, Thoden JB. Biosynthetic enzymes of unusual microbial sugars. Curr Opin Struct Biol. 2010; 20:543–550. [PubMed: 20832292]
25. Terwilliger TC, Berendzen J. Automated MAD and MIR structure solution. Acta Crystallogr D Biol Crystallogr. 1999; 55(Pt 4):849–861. [PubMed: 10089316]
26. Terwilliger TC. Maximum-likelihood density modification. Acta Crystallogr D Biol Crystallogr. 2000; 56(Pt 8):965–972. [PubMed: 10944333]
27. Terwilliger TC. Automated main-chain model building by template matching and iterative fragment extension. Acta Crystallogr D Biol Crystallogr. 2003; 59:38–44. [PubMed: 12499537]
28. Emsley P, Cowtan K. Coot: model-building tools for molecular graphics. Acta Crystallogr D Biol Crystallogr. 2004; 60:2126–2132. [PubMed: 15572765]

29. Murshudov GN, Vagin AA, Dodson EJ. Refinement of macromolecular structures by the maximum-likelihood method. Acta Crystallogr D Biol Crystallogr. 1997; 53:240–255. [PubMed: 15299926]
30. McCoy AJ, Grosse-Kunstleve RW, Adams PD, Winn MD, Storoni LC, Read RJ. Phaser crystallographic software. J Appl Cryst. 2007; 40:658–674. [PubMed: 19461840]
31. Minor W, Cymborowski M, Otwinowski Z, Chruszcz M. HKL-3000: the integration of data reduction and structure solution-from diffraction images to an initial model in minutes. Acta Crystallogr D Biol Crystallogr. 2006; 62:859–866. [PubMed: 16855301]
32. Sheldrick GM, Schneider TR. SHELXL: high-resolution refinement. Methods Enzymol. 1997; 277:319–343. [PubMed: 18488315]
33. Cleland WW. Statistical analysis of enzyme kinetic data. Methods Enzymol. 1979; 63:103–138. [PubMed: 502857]
34. Laskowski RA, MacArthur MW, Moss DS, Thornton JM. *PROCHECK*: a program to check the stereochemical quality of protein structures. J Appl Cryst. 1993; 26:283–291.
35. Vuorio R, Harkonen T, Tolvanen M, Vaara M. The novel hexapeptide motif found in the acyltransferases LpxA and LpxD of lipid A biosynthesis is conserved in various bacteria. FEBS Lett. 1994; 337:289–292. [PubMed: 8293817]
36. Ray WJ Jr, Puvathingal JM. A simple procedure for removing contaminating aldehydes and peroxides from aqueous solutions of polyethylene glycols and of nonionic detergents that are based on the polyoxyethylene linkage. Anal Biochem. 1985; 146:307–312. [PubMed: 4025798]
37. McCarthy TJ, Plog MA, Floy SA, Jansen JA, Soukup JK, Soukup GA. Ligand requirements for glmS ribozyme self-cleavage. Chem Biol. 2005; 12:1221–1226. [PubMed: 16298301]
38. DeLano, WL. The PyMOL Molecular Graphics System. DeLano Scientific; San Carlos, CA, USA: 2002. The PyMOL Molecular Graphics System. DeLano Scientific, San Carlos, CA, USA

Abbreviations

CAPS	(cyclohexylamino)propanesulfonic acid
CHES	2-(cyclohexylaminoethanesulfonic acid)
CoA	coenzyme A
ESI	electrospray ionization
GDP	guanosine diphosphate
HEPPS	N-2-hydroxyethylpiperazine-N′-3-propanesulfonic acid
HPLC	high-performance liquid chromatography
MES	2-(N-morpholino)ethanesulfonic acid
MOPS	3-(N-morpholino)propanesulfonic acid
NMR	nuclear magnetic resonance
PCR	polymerase chain reaction
TEV	tobacco etch virus
Tris	*tris*-(hydroxymethyl)aminomethane

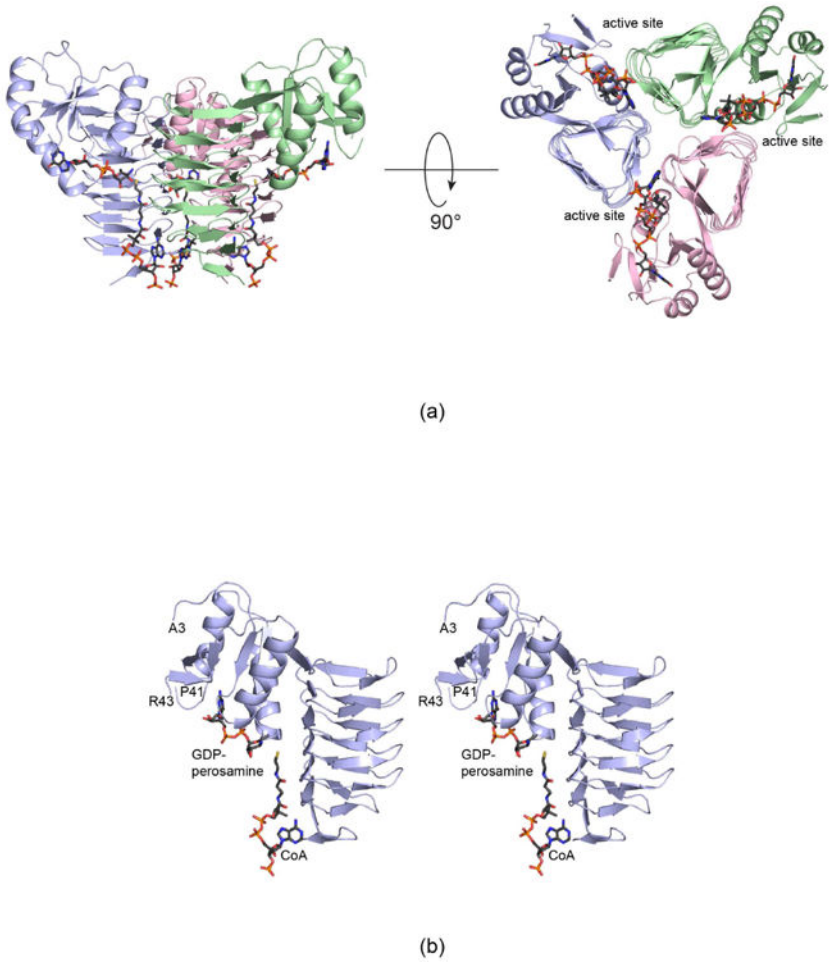

Figure 1.

Ribbon representation of PerB in a complex with CoA and GDP-perosamine. The three subunits of the PerB trimer are highlighted in blue, green, and pink, respectively in (a). The CoA and GDP-perosamine ligands are depicted in stick representations. A close-up view of one subunit of the trimer is displayed in (b). All figures were prepared with the software package PyMOL.[38]

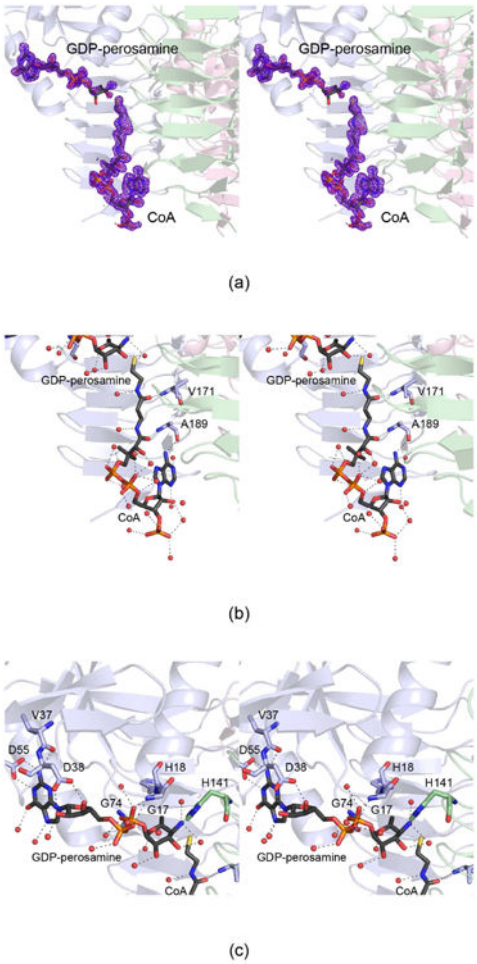

Figure 2.

The PerB active site with bound CoA and GDP-perosamine. The electron densities corresponding to the CoA and GDP-perosamine ligands are displayed in (a). The map, contoured at 3σ, was calculated with coefficients of the form (F_o-F_c) where F_o was the native structure factor amplitude, and F_c was the calculated structure factor amplitude. Close-up views of the CoA and GDP-perosamine binding pockets are depicted in (b) and (c), respectively. Amino acid residues displayed in blue or green belong to different subunits of the trimer. Ordered water molecules are depicted as red spheres. The dashed lines indicate possible hydrogen bonding interactions.

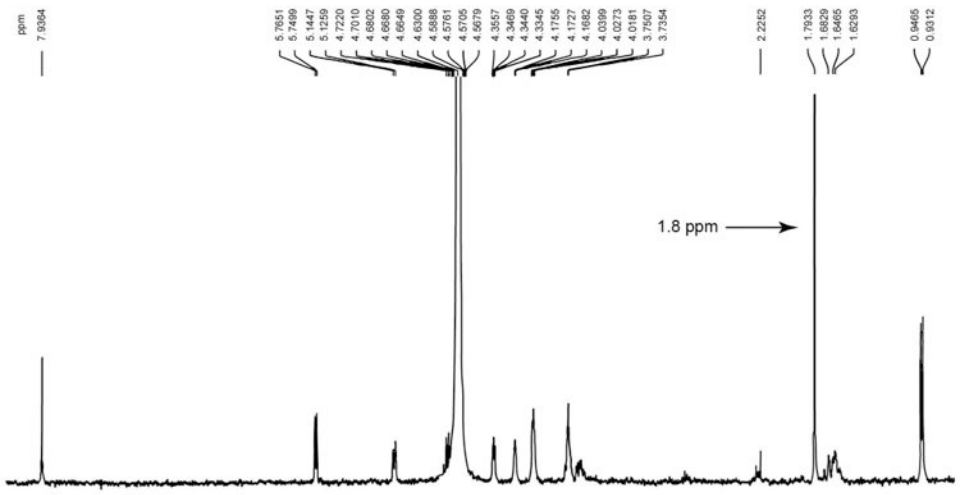

Figure 3.

The ^{1}H NMR spectrum GDP-*N*-acetyl-3-deoxyperosamine. This spectrum corresponds closely to the ^{1}H NMR spectrum for GDP-3-deoxyperosamine, but with the addition of the peak near 1.8 ppm, which is the appropriate chemical shift for protons in an *N*-acetyl group.

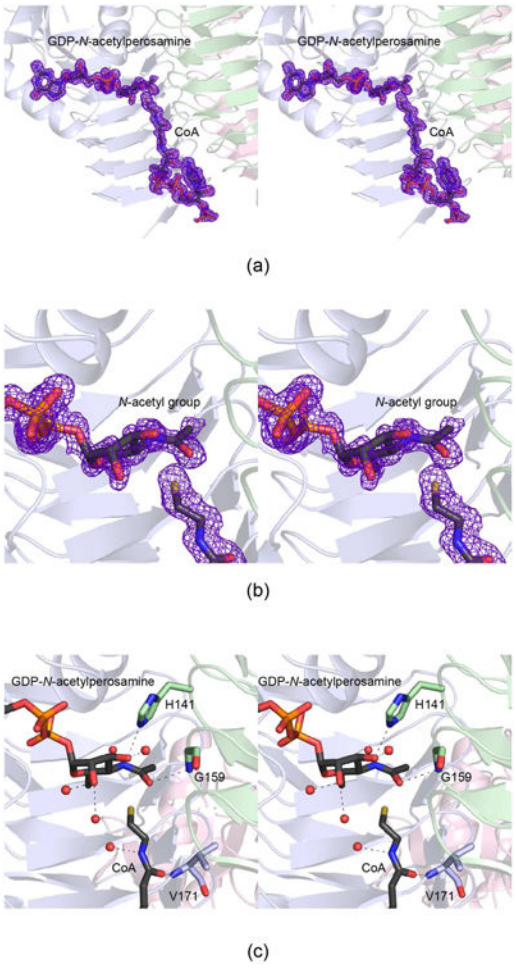

Figure 4.

The PerB active site with bound CoA and GDP-*N*-acetylperosamine. The electron densities corresponding to CoA and the nucleotide-linked sugar are presented in (a). The map was calculated as described in Figure 2, and contoured at 3.5σ. A close-up view of the acetylated sugar product is provided in (b). Possible hydrogen bonding interactions between the *N*-acetylated sugar product and the protein are depicted as dashed lines in (c).

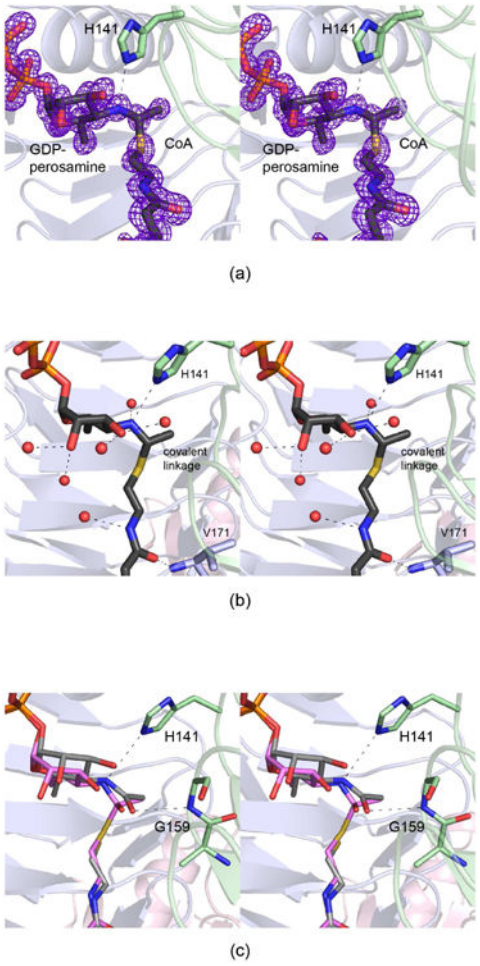

Figure 5.

The PerB active site with a CoA/GDP-perosamine covalent adduct. The electron density corresponding to the covalent adduct is displayed in (a). The map was calculated as described in Figure 2, and contoured at 3.5σ. Possible hydrogen bonding interactions between the ligand and the protein are indicated by the dashed lines in (b). Ordered water molecules are displayed as spheres. A superposition of GDP-*N*-acetylperosamine (gray filled bonds) onto the covalent adduct (pink filled bonds) is depicted in (c).

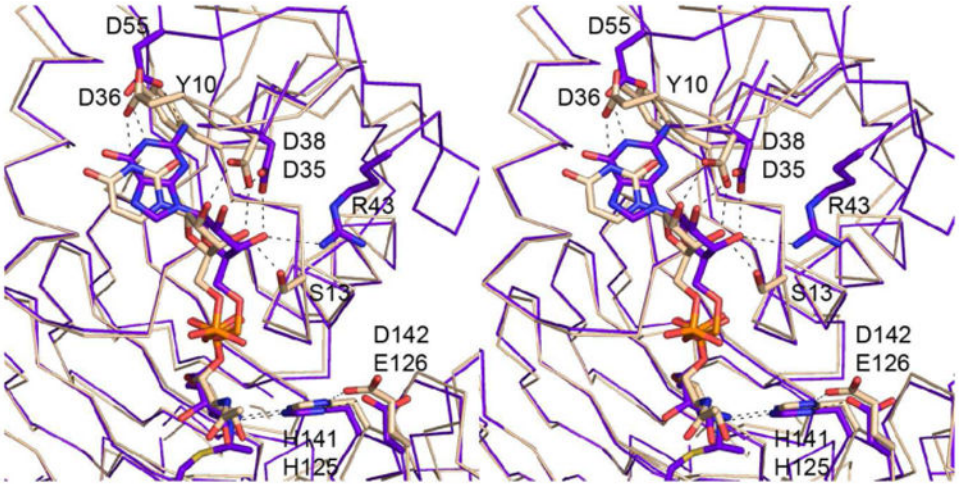

Figure 6.

Comparison of the PerB and PglD active sites. The ribbon traces of PerB and PlgD are colored in purple and wheat, respectively. The ligand and side chains belonging to PerB are displayed in purple filled bonds, whereas those for PlgD are highlighted in wheat bonds. In the case where there are two amino acid residues labeled, the top one corresponds to PerB and the bottom to PglD. Possible hydrogen bonds are indicated by the dashed lines.

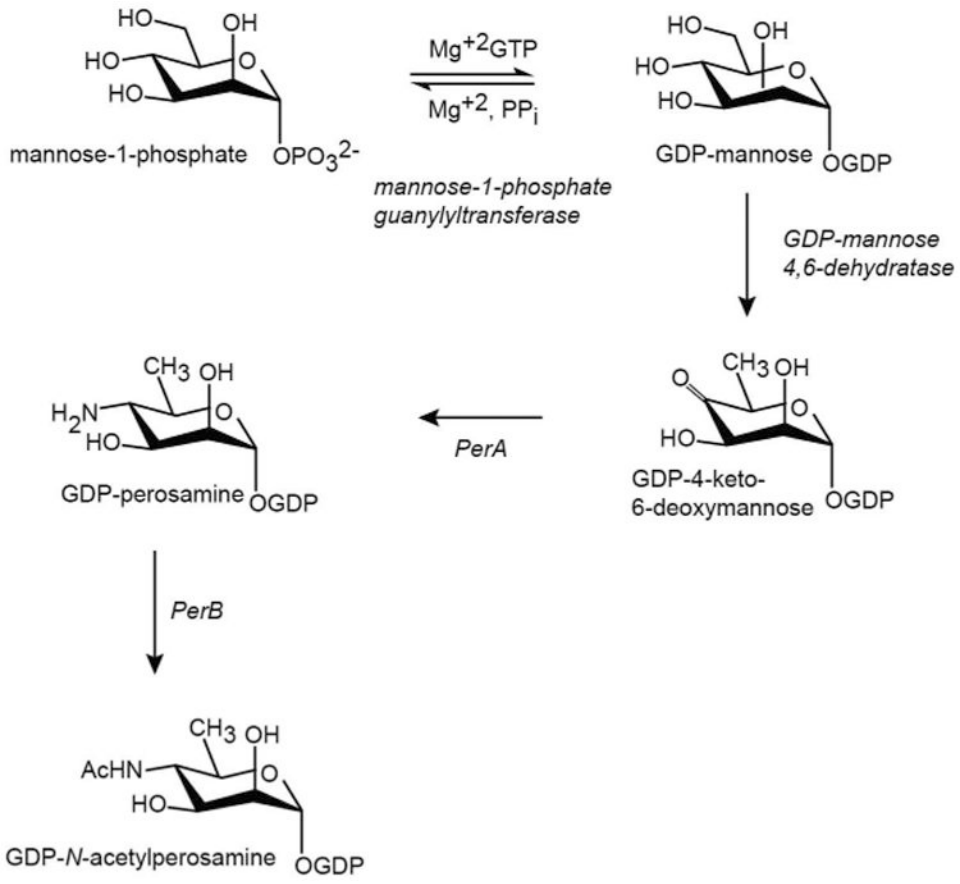

Scheme 1.

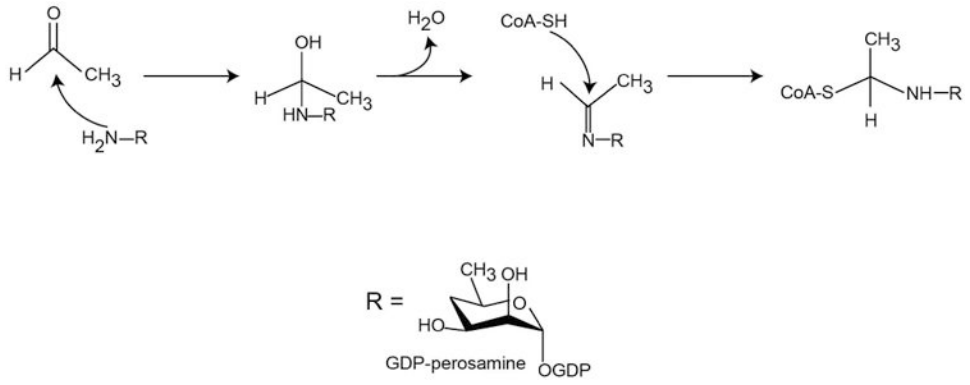

Scheme 2.

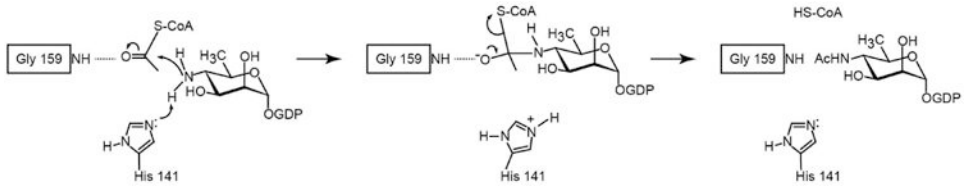

Scheme 3.

Table 1

X-ray Data Collection Statistics.

	PerB/CoA/GDP-perosamine	PerB/CoA/GDP-*N*-acetylperosamine	PerB/CoA/GDP-perosamine adduct	H141N/GDP-perosamine	H141A/GDP-perosamine
resolution limits	50.0-1.0 (1.02-1.0)[b]	50.0-1.0 (1.02-1.0)	50.0-0.90 (0.92-0.90)	50.0-1.45 (1.55-1.45)	50.0-1.35 (1.44-1.35)
number of independent reflections	132706 (6420)	132601 (6425)	181485 (8807)	44567 (8131)	53728 (8988)
completeness (%)	98.3 (95.4)	98.5 (95.8)	98.6 (95.9)	99.2 (97.4)	97.2 (93.4)
redundancy	7.3 (3.3)	7.2 (3.3)	8.1 (3.6)	9.3 (4.3)	6.5 (3.0)
avg I/avg σ(I)	44.8 (2.3)	47.1 (2.0)	50.6 (2.4)	14.5 (2.9)	16.4 (2.1)
R_{sym} (%)[a]	6.8 (37.4)	6.3 (39.1)	7.2 (36.0)	6.6 (36.4)	5.3 (39.1)

[a] $R_{sym} = (\Sigma|I - \bar{I}|/ I) \times 100$.

[b] Statistics for the highest resolution bin.

Table 2

Refinement Statistics.

	PerB/CoA/GDP-perosamine	PerB/CoA/GDP-*N*-acetylperosamine	PerB/CoA/GDP-perosamine adduct	H141N/GDP-perosamine	H141A/GDP-perosamine
space group	I23	I23	I23	I23	I23
unit cell dimensions (Å)	114.9	115.5	115.8	115.0	115.0
resolution limits (Å)	50-1.0	50.0-1.0	50.0-0.90	50.0-1.45	50.0-1.35
[a]*R*-factor (overall)%/no. reflections	15.2/132551	14.4/132447	13.9/181331	18.1/43437	18.8/53728
R-factor (working)%/no. reflections	15.1/125918	14.2/125820	13.8/172255	17.9/41237	18.7/50998
R-factor (free)%/no. reflections	17.5/6633	16.6/6627	15.5/9076	21.0/2200	20.4/2730
number of protein atoms	1487[b]	1517[c]	1495[d]	1504[e]	1497[f]
number of heteroatoms	364[g]	421[h]	434[i]	288[j]	317[k]
average B values					
protein atoms (Å^2)	14.1	15.0	11.9	14.0	14.5
ligands (Å^2)	24.6	20.5	14.6	27.8	23.3
solvent (Å^2)	34.1	38.4	33.2	26.4	27.7
weighted RMS deviations from ideality					
bond lengths (Å)	0.016	0.015	0.015	0.012	0.012
bond angles (°)	2.41	2.45	2.29	2.11	2.10
general planes (Å)	0.010	0.011	0.009	0.011	0.010

[a] *R*-factor = $(\Sigma|F_O - F_C| / \Sigma|F_O|) \times 100$ where F_O is the observed structure-factor amplitude and F_C is the calculated structure-factor amplitude.

[b] These include multiple conformations for Ile 12, Ser 25, Arg 77, Lys 81, Ser 92, Met 116, Ile 133, Asp 140, and Arg 174.

[c] These include multiple conformations for Ile 12, Glu 31, Asp 75, Lys 81, Arg 84, Ser 92, Arg 108, Glu 165, Arg 174, Lys 209, and Lys 211.

[d] These include multiple conformations for Ile 12, Asp 75, Arg 77, Lys 81, Ser 92, Ile 133, Leu 151, Ser 155, Ser 162, Arg 174, and Lys 209.

[e] These include multiple conformations for Ser 25, Thr 32, Asp 75, Arg 77, Met 116, Trp 126, and Asp 140.

[f] These include multiple conformations for Ile 12, Lys 20, Thr 32, Asp 75, and Arg 77.

[g] These include 1 CoA, 1 GDP-perosamine, 2 chloride ions, and 277 waters.

[h] These include 1 CoA, 1 GDP-*N*-acetylperosamine, 2 chloride ions, and 330 waters.

[i] These include 1 CoA-GDP-perosamine adduct, 3 chloride ions, and 343 waters.

[j] These include 1 CoA, 1 GDP-perosamine, 1 chloride ion, 1 sodium ion, and 200 waters.

[k] These include 1 CoA, 1 GDP-perosamine, 1 chloride ion, 1 sodium ion, and 229 waters.

Table 3

Kinetic Parameters Measured at pH 8.0.

Protein	K_m (mM) GDP-perosamine	K_m (mM) acetyl CoA	k_{cat}/K_m ($M^{-1}s^{-1}$) GDP-perosamine
Wild-type	0.087 ± 0.011	0.15 ± 0.02	3.5×10^6
H141N	0.15 ± 0.01	0.094 ± 0.017	2.1×10^2
H141A	0.20 ± 0.01	0.11 ± 0.01	2.0
D142N	0.11 ± 0.01	0.059 ± 0.007	3.5×10^5

Table 4

Kinetic Parameters Measured from pH 6.0 to 11.0.

Protein	pH					
	6.0	**7.0**	**8.0**	**9.0**	**10.0**	**11.0**
Wild-type[a,b]	0.27 ± 0.03 1.9×10^4	0.32 ± 0.05 4.3×10^5	0.087 ± 0.011 3.5×10^6	0.21 ± 0.03 2.3×10^6	0.84 ± 0.06 6.9×10^5	9.7 ± 0.4 9.6×10^4
H141N	7.2 ± 0.3 2.0	0.27 ± 0.04 4.1×10^1	0.15 ± 0.01 2.1×10^2	0.097 ± 0.006 4.3×10^2	0.32 ± 0.03 2.5×10^2	6.5 ± 1.7 2.5×10^1
H141A	nd[c]	nd	0.20 ± 0.01 2.0	nd	nd	nd
D142N	0.39 ± 0.05 8.4×10^3	0.30 ± 0.03 8.0×10^4	0.11 ± 0.01 3.5×10^5	0.074 ± 0.004 3.9×10^5	0.27 ± 0.04 1.6×10^5	3.5 ± 0.3 4.2×10^4

[a] K_m (mM) GDP-perosamine, top line

[b] k_{cat}/K_m ($M^{-1}s^{-1}$), bottom line

[c] not determined

Table 5

pK_a Values Determined from pH Rate Profiles

Protein	pK_{a1}	pK_{a2}	pK_{a3}
Wild-type[a]	7.8 ± 0.3	9.3 ± 0.2	6.5 ± 0.5
H141N[a]	8.1 ± 0.2	9.7 ± 0.2	6.0 ± 0.5
D142N[b]	7.7 ± 0.1	9.9 ± 0.1	

[a] Fit with BEL2L

[b] Fit with BELL